Energy damage index based on capacity and response spectra

S.A. Diaz[1,3], L.G. Pujades[1], A.H. Barbat[2], Y.F. Vargas[1], D.A. Hidalgo-Leiva[1]*

[1]Polytechnic University of Catalonia (UPC), DECA-ETCG, Barcelona Tech, Spain.
[2]Polytechnic University of Catalonia (UPC), DECA-MMCE, Barcelona Tech, Spain.
[3] Universidad Juárez Autónoma de Tabasco (UJAT), DAIA, Tabasco, Mexico.

ABSTRACT

Non-linear dynamic analysis and the damage index of Park-Ang have been often used to assess expected seismic damage to a structure. Depending on the size of the structure and the duration of the record, the computational effort in dynamic analyses is usually high. In this research, a new damage index is proposed based on nonlinear static analysis. The damage index is a linear combination of two energy functions: 1) the strain energy associated with the stiffness variation and the ductility of the structure, and 2) the dissipated energy associated with hysteretic cycles. These two energy functions are obtained from the capacity curve of the structure and from the energy balance with the spectral acceleration. To show the ability of the index to represent damage, low-rise steel buildings were studied under the seismic actions that are expected in Mexico City. The results obtained with the new method show good agreement with those calculated by means of dynamic analyses using the Park-Ang damage index. On average, the Park-Ang damage index is well-fitted by the combination of 62% of the strain energy and 38% of the energy dissipated by hysteresis. Moreover, the new damage index can link damage to certain characteristics of seismic actions, such as their intensity and duration. Therefore, the new approach results in a practical, powerful tool for estimating seismic damage in buildings, especially as probabilistic approaches require massive computations.

Keywords: capacity curve, damage assessment, strain energy, energy dissipated by hysteresis, Monte Carlo simulations

1 Introduction

In assessments of the seismic performance of buildings, non-linear dynamic analysis (NLDA) has proved to be the most realistic, suitable, sophisticated, numerical tool to estimate the response of a structure as a function of time. When NLDA is used to assess the seismic response, the input is generally a group of accelerograms that can be recorded, synthetic or both. If NLDA is performed by increasing the ordinates of the selected accelerograms, it is known as incremental dynamic analysis (IDA) [1]. IDA can be used to obtain curves relating a measure of the seismic response of a structure (displacement at the roof, maximum inter-story drift, etc.) to a variable that describes seismic intensity, such as peak ground acceleration (PGA). The IDA has been used as the most appropriate tool for assessing damage in structures subjected to dynamic actions [1]. Several damage indices can be calculated from the dynamic response of a structure [2,3], and are related to a reduction in the capacity of buildings' structural elements. Some studies have proposed damage indices for reinforced concrete and steel buildings, considering parameters

such as displacement ductility [4,5], strength and stiffness degradation [3], energy dissipation [6,7], cyclic fatigue [8], change in the natural period of the structure [9], or a combination of the above parameters [10–13]. Most of the damage indices proposed to date take values in the range of 0 to 1, where 0 indicates no damage and 1 collapse. Park and Ang [11] proposed one of the most frequently used seismic damage indices for reinforced concrete buildings, which considers both the maximum structural response and the cyclic load effect [14–16].

Considerable computational effort is required to calculate damage curves based on IDA. To avoid this effort, non-linear static analysis (NLSA) offers an interesting alternative due to its simplicity [17,18], but the results must be in good agreement with those provided by IDA. Several researchers have employed NLSA to estimate parameters related to the dynamic response of structures [19–23] or in risk studies at urban level [24–27]. In the present article, a new damage index for steel buildings is proposed that can be obtained from the capacity curve. It fits well with the damage index of Park and Ang. The mathematical formulation of the new damage index is based on energy functions and on the idea proposed by Pujades et al. [22] of using a calibration parameter to determine the contribution to damage of two or more simple functions and, thus, to obtain good agreement with a relatively more complex damage index. Nevertheless, new functions that consider two types of energy from the capacity curve are used herein: 1) strain energy and 2) energy dissipated by hysteresis [28,29]. When both functions are combined, a new damage index is obtained that is compatible with that of Park and Ang. In order to consider the effect of the seismic hazard, the performance point is based on the concept of energy balance [30] and the application of the seismic evaluation is based on the study by Leelataviwat et al. [31]. A three-storey steel building under the seismic actions expected in Mexico City was used as the test bed. First, a deterministic case is presented to formulate the new damage index. A probabilistic approach based on the Monte Carlo method and on the Latin hypercube sampling (LHS) technique is also included. The cases studied in this article show that the new damage index for the type of steel structures analysed herein can be used to assess expected damage directly from the capacity curve, in a straightforward way, thus avoiding the considerable computational effort involved in dynamic simulations.

2 Damage model based on energy

2.1 Damage index of Park and Ang

The damage index of Park and Ang [11] can be used to estimate the damage level of structures, starting from a post-process of the nonlinear dynamic response. It is calculated as the sum of the maximum displacement, divided by the ultimate displacement with a term related to the dissipated energy. For a structural element, the damage index, $DIe_{PA}(\delta)$, is given by the following equation:

$$DIe_{PA}(\delta) = \frac{\delta}{\delta_u} + \frac{\beta}{Q_y \delta_u} \int_0^{\delta} dE \tag{1}$$

where δ/δ_u is the ductility defined as the ratio of the maximum displacement of the structural element subjected to a specific earthquake, δ, to the ultimate displacement under monotonic loading, δ_u. Qy is the strength at the yielding

point. If the strength, Qu, corresponding to the ultimate displacement, δu, is lower than Qy, then Qy is substituted by Qu. $\int_0^{\delta} dE$ represents the hysteretic energy absorbed by the element during the earthquake and β is a non-negative strength deteriorating parameter. The overall damage index of a structure is obtained by calculating the weighted damage index, $DI_{PAw}(\delta)$. The following equation was proposed by Park and Ang [11] in order to calculate $DI_{PAw}(\delta)$:

$$DI_{PAw}(\delta) = \sum_{i=1}^{N} \lambda_i DIe_{PA}(\delta)_i \quad (2)$$

where $DIe_{PA}(\delta)_i$ is the damage index of structural element I as defined in Equation (1), N is the number of damaged elements, and λ_i is the ratio of the energy dissipated by hysteresis in element i to the total hysteretic energy dissipated in the entire structure. Values of the damage index above 1.0 indicate structural collapse. In this article, the Park and Ang damage index is used as a reference for the validation of the new damage index proposed herein. The new damage index is based on the concepts of ductility and energy dissipated by hysteretic cycles, which are similar to those considered in the Park and Ang index

2.2 The proposed damage index

Chopra [32] showed that the damping exhibited when the earthquake ground motion drives a structure into the inelastic range can be viewed as a combination of viscous damping, inherent to the structure, and hysteretic damping. Hysteretic damping is related to the area inside the loops defined by earthquake force–structural displacement diagrams. Hysteretic damping can be represented as equivalent viscous damping, ξ_{eq}, associated with a maximum displacement, and it can be estimated by means of the following equation [32]:

$$\xi_{eq} = \frac{1}{4\pi}\frac{E_D}{E_{so}} \quad (3)$$

where E_{so} is the maximum strain energy associated with a cycle of motion, that is, the area under the secant stiffness at the ultimate point (D_{ci}, F_{ci}) of the capacity curve, which can be calculated as:

$$E_{so} = \frac{(Dci * Fci)}{2} \quad (4)$$

E_D is the energy dissipated by the structure in a single cycle of motion, that is, in a single hysteretic loop. A graphic representation of E_D and E_{so} is shown in

Figure 1. E_D can be calculated starting from the bilinear representation of the capacity curve as the area enclosed within a single hysteretic loop, equivalent to the area of the large parallelogram shown in

Figure 1.

The bilinear representation is obtained as follows: i) the area under the bilinear curve must be equal to the area under the original capacity curve, Ac; ii) the initial slope, Ki, must be equal in both curves; and iii) the coordinates

of the ultimate capacity point (D_{ci}, F_{ci} and D_{bi}, F_{bi}) must match both curves. Based on the latter conditions, the following equations can be used to calculate the coordinates of the yield point (Dy, Fy):

$$D_y = \frac{2\,Ac - (F_{ci} * D_{ci})}{(K_i * D_{ci}) - F_{ci}} \tag{5}$$

$$F_y = (K_i * D_y) \tag{6}$$

Starting from the points defined by the bilinear curve, E_D is calculated using the following equation [28,32]:

$$E_D = 4(F_y * D_{bi} - D_y * F_{bi}) \tag{7}$$

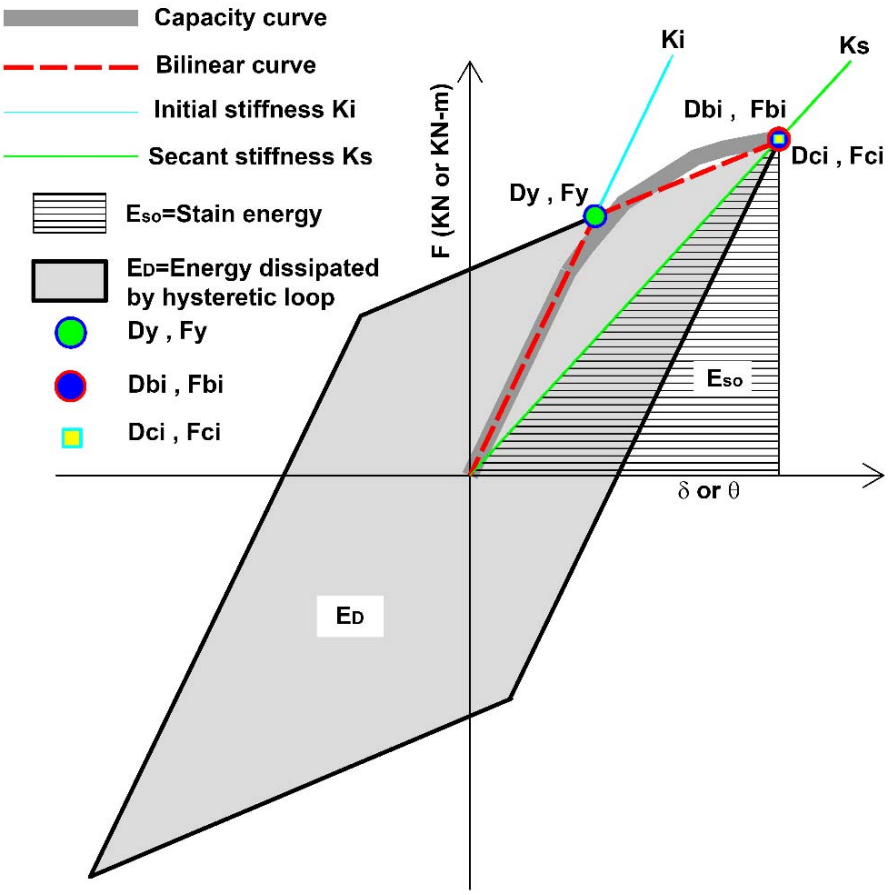

Figure 1. Capacity curve, bilinear curve (force–deformation relation) and equivalent viscous damping due to hysteretic energy dissipation.

Note that E_{so} and E_D can be calculated from the capacity curve as a function of the displacement at the roof δ, in an incremental manner. Thus, two energy functions are defined as follows: 1) strain energy function, $E_{so}(\delta)$ and 2) energy dissipated by hysteretic function, $E_D(\delta)$. Based on the mathematical development of Chopra [32] for $E_{so}(\delta)$ and $E_D(\delta)$, the former can be related to stiffness and ductility, and the latter to energy dissipation; both functions depend on the intensity of the earthquake.

Based on these functions, a damage index can be derived by adopting the two following criteria.: i) both functions are normalized to 1 for the value related to the ultimate displacement, δu, of the capacity curve; ii) both functions will have a value equal to zero for $\delta \leq \delta_{Dy}$ because, within the linear range of the structure, the expected damage should be zero. Thus, the normalized energy functions $E_{so}(\delta)_{NN}$ and $E_D(\delta)_{NN}$ can be calculated by means of the following equations:

$$E_{so}(\delta)_{NN} = \begin{cases} 0 & 0 \leq \delta \leq \delta_{D_y} \\ \dfrac{E_{so}(\delta)}{E_{so}(\delta_u)} & \delta_{D_y} < \delta \leq \delta_u \end{cases}, 0 \leq E_{so}(\delta)_{NN} \leq 1 \quad (8)$$

$$E_D(\delta)_{NN} = \begin{cases} 0 & 0 \leq \delta \leq \delta_{D_y} \\ \sum_{j=0}^{n} E_D(\delta) \Big/ \left[\sum_{j=0}^{n} E_D(\delta)\right]_{max} & \delta_{D_y} < \delta \leq \delta_u \end{cases}, 0 \leq E_D(\delta)_{NN} \leq 1 \quad (9)$$

where *j* represents each increment in the displacement of the capacity curve, *n* represents the ultimate increment. Using equations 8 and 9, the following damage index, $DI_{EC}(\delta)$, is then proposed:

$$DI_{EC}(\delta) = \eta E_{so}(\delta)_{NN} + (1 - \eta) E_D(\delta)_{NN} \cong DI_{PAw}(\delta) \quad (10)$$

Observe that $DI_{PAw}(\delta)$ can be used to calibrate the value of parameter η. Parameter η is directly related to how much the strain energy function contributes to the damage (as a percentage), while its counterpart in Eq.10 corresponds to how much the energy dissipated due to the hysteretic function contributes to the damage. The two energy functions can be obtained from the capacity curve of the building. However, they can also be obtained from the bending moment M rotation θ curve of a structural element. $DIe_{PA}(\delta)$ is used to calibrate the value of the parameter η. This new damage index is referred to hereinafter as the energy capacity damage index, $DI_{EC}(\delta)$. The calculation and implementation of $DI_{EC}(\delta)$ are presented in the next section.

3 Example of implementation the new damage index

3.1 Structural model

A three-storey steel building with four spans is used to illustrate the computation of the proposed energy capacity damage index. This building has been studied extensively by Diaz et al. [33,34] to assess its performance and expected seismic damage under conditions in Mexico City. The main geometric characteristics and structural sections of the building are shown in Figure 2. The structural system of the building is a special moment frame (SMF), composed of beams and columns with W sections (American wide flange section) that are joined by means of prequalified connections [35] of a fully restrained (FR) type. This structure was designed as an office building, considering the provisions of NTC-DF [36] and ANSI/AISC 341-10 [37]. The design of the SMFs satisfies the criterion of strong column-weak beam. Both static and dynamic nonlinear structural analyses were performed using

Ruaumoko 2D software [2]. Beams and columns were modelled as FRAME type members, with plastic hinges at their ends. The plastic hinges follow the bi-linear hysteresis rule. The hardening and strength reduction were calculated, based on the ductility factor (see Appendix A - Ruaumoko 2D [2]). Due to limitations of the adopted model, which only reproduces the failure by bending moment, the interaction between the bending moment and the axial force has not been considered. Obviously, most of the damage of this type of building is expected to occur at the ends of the elements, mainly because the effects of the bending moment. The values of strength and ductility were calculated according to the modified Ibarra–Medina–Krawinkler (IMK) model [38–40]. The panel zones were modelled using the rotational stiffness in connections, according to the model of Krawinkler [41] included in FEMA 355C [42]. For the damping, the Rayleigh model is assumed and a damping ratio of 2% [43,44]. The fundamental period, T_1, of the building model is 0.63 s.

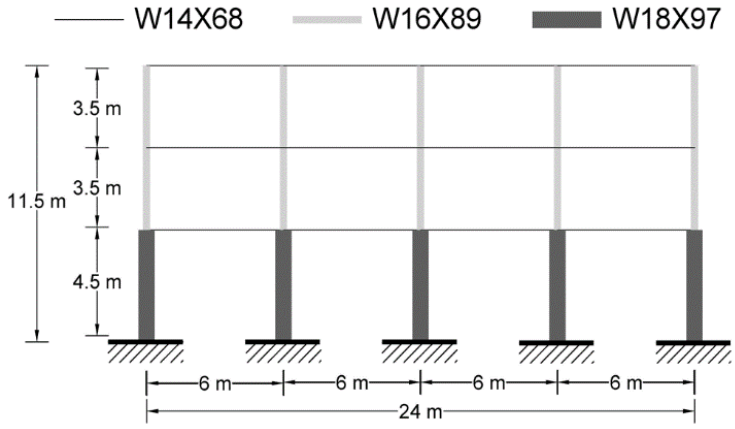

Figure 2. Geometry and structural section of the archetype building.

3.2 Seismic actions

Damage curves must be obtained using the IDA method to calibrate the new damage index, $DI_{EC}(\delta)$. Acceleration records of Mexico City were used in this example. The design spectrum for the IIIa seismic area, according to NTC-DF [36], was taken as a target spectrum. The selection method proposed by Vargas et al. [21] was applied to a database containing 2554 accelerograms recorded in the Mexico City area [45]. Four accelerograms were thus selected whose mean response spectra are compatible with the target spectrum. The main characteristics of these accelerograms are shown in Table 1.

Table 1. Characteristic of the seed accelerograms used in seismic zone IIIa in Mexico City.

Acc.	Station	Date	Duration (seconds)	Epicentre			Magnitude (Mw)	Component	PGA (cm/s2)	Epicentre distance (km)	Azimut Sta-Epi
				Latitude	Longitude	Depth (Km)					
1	**AL01**	18/04/2014	165.77	17.18 N	101.19 W	10	7.2	S00E	28.86	330.89	221.04
2	**HJ72**	18/04/2014	167.47	17.18 N	101.19 W	10	7.2	N90W	32.19	331.06	221.39
3	**MJSE**	15/06/1999	144.01	18.18 N	97.51 W	69	7.0	N76W	13.76	222.31	128.79
4	**TL55**	30/09/1999	173.86	15.95 N	97.03 W	16	5.2	N90E	15.62	447.59	149.67

Each one of the accelerograms in Table 1 was used as a seed within a probabilistic spectral matching technique [33,46] to obtain 5 new accelerograms whose response spectra show good agreement with the target spectra. Thus, a set of 20 matched accelerograms was obtained, which were considered suitable to deal with uncertainties in the seismic actions, to validate the proposed damage index in a probabilistic environment. Figure 3a shows the seed accelerogram 1 and one of the matched accelerograms that was used to perform the IDA analysis. Figure 3b shows the target spectrum, the response spectrum of seed accelerogram 1 and the response spectrum of the matched accelerogram.

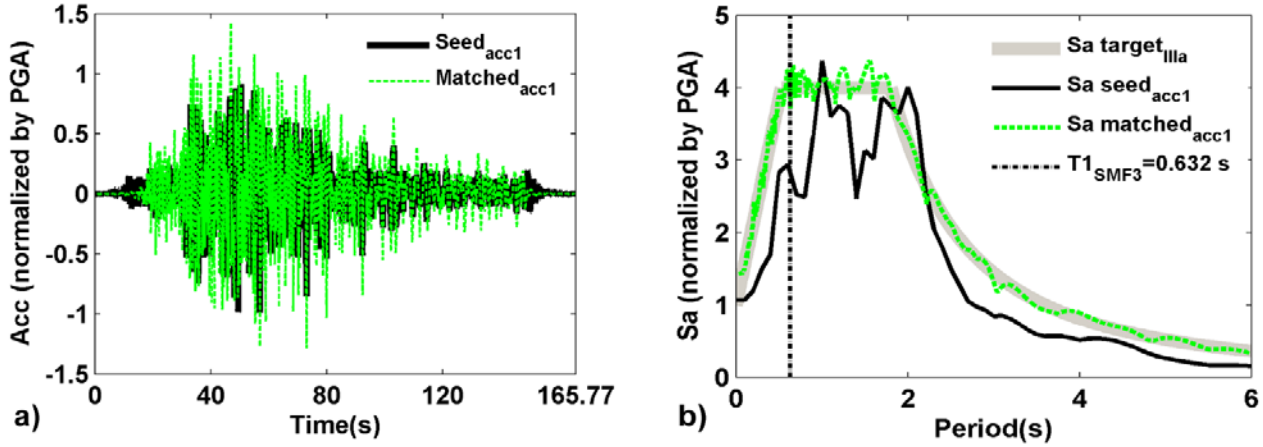

Figure 3. a) The seed accelerogram 1 and the matched accelerogram, and b) the target spectrum (IIIa) and the response spectra for seed accelerogram 1 and the matched accelerogram.

3.3 Capacity curve

The capacity curve was obtained by means of an adaptive pushover analysis (PA), implemented in Ruaumoko software [2]. This method is independent of the initial loading pattern, as it adapts the pattern at each step of the PA, according to the shape of the first vibration mode of the structure. The ultimate capacity is established when one of the following criteria is fulfilled: i) ω^2 is less than 10^{-6} ω^2 at the first step, where ω is the tangent fundamental natural frequency in the Modified Rayleigh Method; ii) the Newton Raphson iteration is not achieved within a maximum number of specified cycles; iii) the stiffness matrix becomes singular; and iv) a specified maximum structure displacement is reached. In the NLSAs of the studied models, many cycles of the Newton Raphson method were considered. Moreover, a large maximum limit for structure displacement was considered. Thus, the failure criteria are expected to be related to criteria i or iii. The conventional pushover analysis and the adaptive pushover analysis, P_{ad}, for buildings with structural response dominated by their fundamental mode provide similar capacity curves; however, in this research, the P_{ad} was preferred, because it includes predefined criteria to determine the ultimate capacity point. This aspect is useful in probabilistic assessments to define the collapse for each analysis. Moreover, these failure criteria, predefined in the capacity curve, allow improving compatibility with the ultimate capacity achieved in the IDA. However, conventional pushover can be also used if the ultimate capacity point is adequately defined. Figure 4a shows the plastic hinges corresponding to the ultimate capacity point of the building

and Figure 4b shows the respective inter-story drift. The level of plasticization of each plastic hinge is measured respect to its plastic rotation limit, when the building reaches its ultimate capacity. Finally, Figure 5a shows the capacity curve that was obtained.

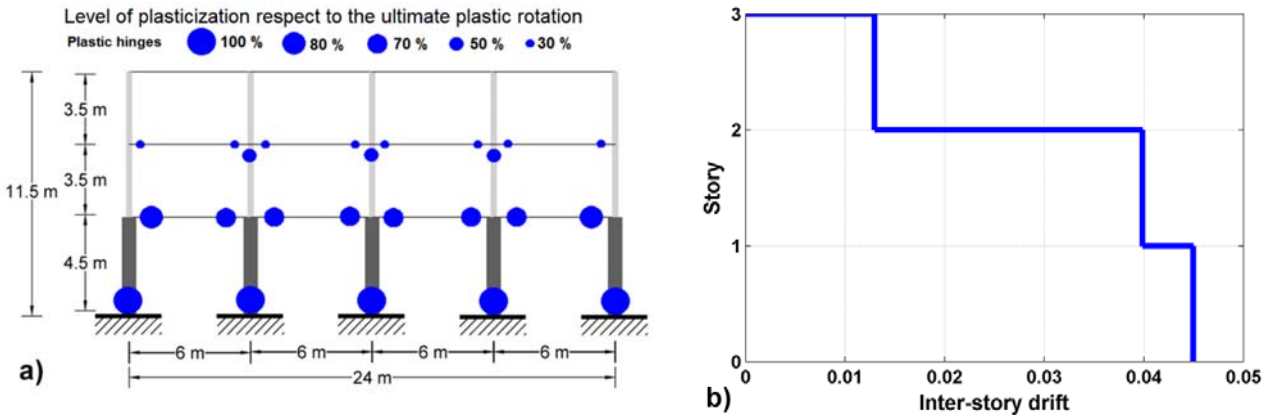

Figure 4 a) Plastic hinges formed when the building reaches its ultimate capacity and b) the corresponding inter-story drift.

3.4 Incremental dynamic analysis

Incremental dynamic analysis was performed for the building using the matched accelerogram shown in Figure 3a. The PGA of the record was increased until the collapse of the structure, established in terms of ultimate displacement δ_u. In this case, the collapse displacement of the building corresponds to a PGA of 1 g. The $DI_{PAw}(\delta)$ function of the roof displacement, δ, for the building is shown in Figure 5a. The capacity curve and the $DI_{PAw}(\delta)$ were used in subsequent sections to calibrate the new damage index.

In order to prove that the new damage index could also be applied to a structural element, the following were extracted using the IDA results for the building: i) the relation between $DIe_{PA}(\theta)$ and the rotation θ, and ii) the bending moment M–rotation θ curve of one of the beams on the first floor in the building, which is referred to hereinafter as BEAM 1 and shown in Figure 5b.

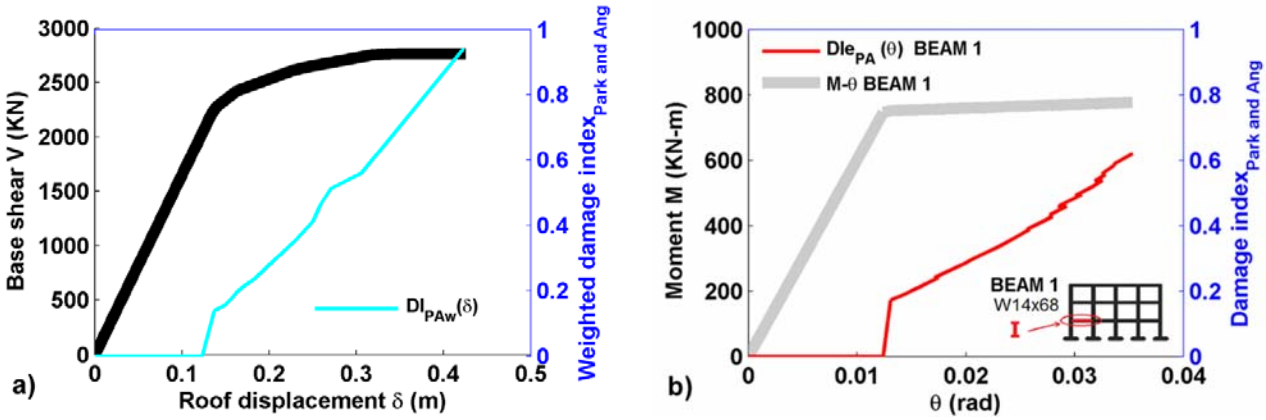

Figure 5. a) Capacity curve and the $DI_{PAw}(\delta)$ by IDA of the building; and b) the $DIe_{PA}(\theta)$ and M-θ diagram of the BEAM 1.

3.5 Proposed energy damage index for a structural element

As a first step, the damage index was implemented for a structural element, so that it could be calibrated with $DIe_{PA}(\theta)$. This was performed for the structural element, BEAM 1. Based on the M-θ curve, the two energy functions depending on the angular deformation, $E_{so}(\theta)_{NN}$ and $E_D(\theta)_{NN,}$ were obtained (see Figure 6). Then, the energy capacity damage index for a structural element, $DI_{EC}(\theta)$, was calibrated by considering the $DIe_{PA}(\theta)$. The parameter η was obtained by means of least squares fit of Eq 10. For the case discussed herein, the parameter η was set to 0.78. The contribution to the damage index of the strain energy function, $E_{so}(\theta)_{NN}$, was 78%, while the contribution of the energy dissipated by hysteretic, $E_D(\theta)_{NN}$, was 22%. Figure 6 shows the $DIe_{PA}(\theta)$ and $DI_{EC}(\theta)$ for BEAM 1. $DI_{EC}(\theta)$ was in excellent agreement with $DIe_{PA}(\theta)$. The parameter η allowed a good fit of the new index, $DI_{EC}(\theta)$, to the expected damage in a structural element subjected to seismic actions.

This example shows that the proposed functions and damage index can replicate the Park and Ang damage index in the structural elements. However, the proposed index is also a viable alternative to reduce the computational time in the probabilistic assessments if it is obtained directly from the capacity curve, as shown in the next section.

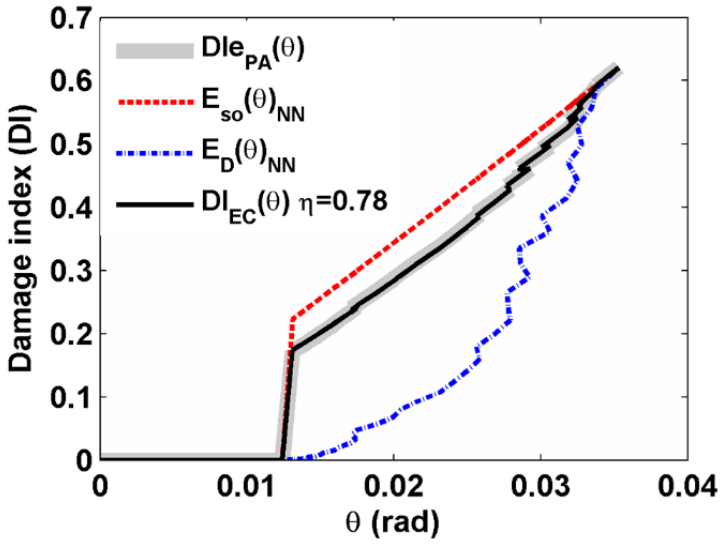

Figure 6. New damage index of $DIe_{EC}(\theta)$ and $DI_{PA}(\theta)$ for BEAM 1.

3.6 Energy capacity damage index for the entire building

To calibrate the simplified energy capacity damage index $DI_{EC}(\delta)$, it was considered that the evolution of damage $DI_{PAw}(\delta)$ is closely related to the roof displacement caused by the seismic action. These displacements are expected to differ for different seismic actions, because important properties such as the duration and frequency content of each seismic action may vary, causing a different structural response for equal PGA values.

The IDA method provides the displacement pattern as a function of the PGA. Otherwise, in NLSA, the performance point for each PGA value must be calculated in order to define the roof displacements as a function of the increased PGA of seismic action, $Sd_{pp}(PGA)$. The performance point can be obtained by applying the capacity spectrum

method proposed by Freeman [47] and included in ATC-40 [28], FEMA-273 [48]. Chopra and Goel [29] and Fajfar [49,50] developed an improved version of the capacity spectrum method that uses the constant-ductility design spectrum as a demand diagram. In these studies, the concepts of equivalent ductility factors by the R_y-μ_s-T equations introduced by Newmark and Hall [51] and Vidic et al. [52] are used, where R_y is the reduction factor due to ductility, μ_s is the ductility factor defined as the ratio between the maximum displacement and the yield displacement, and T is the period of the demand spectrum. Another proposal for calculating the performance point is that of Mezzi et al. [53] and Leelataviwat et al. [31,54], which is based on the balance between the energy spectrum of the seismic action in the energy displacement response spectrum (EDRS) format and the energy obtained from the area beneath the capacity curve, named accumulated deformation energy (ADE). In the present research, the energy balance method was used to obtain displacement patterns due to seismic actions. In this method, the capacity curve obtained from the building, shown in Figure 5a, and the response spectrum of the acceleration shown in Figure 3b, were used.

The first step for calculating the performance point consisted of obtaining the accumulated deformation energy, ADE, of the capacity curve, F(δ), using the following equation:

$$\mathrm{ADE}(\delta) = \int_0^{\delta} \mathrm{F}(\xi)\mathrm{d}\xi \qquad 0 \leq \xi \leq \delta_u; \qquad 0 \leq \mathrm{ADE}(\delta) \leq \mathrm{ADE}(\delta_u) \tag{11}$$

Figure 7 shows the capacity curve and the ADE(δ) curve of the building. The yielding roof displacement, δ_y, the yielding base shear, V_y, and the yielding energy E_y are also plotted in this figure. The second step consisted of obtaining the input energy spectrum in EDRS format ($\mathrm{Sa_{EDRS}}$) from the pseudo-velocity spectrum, Sv, using the following equation:

$$\mathrm{Sa_{EDRS}} = \frac{1}{2}\gamma_E \mathrm{M^*Sv^2} = \frac{1}{2}\gamma_E \mathrm{M^*Sa^2}\left(\frac{\mathrm{T}}{2\pi}\right)^2 \tag{12}$$

$$\gamma_E = \frac{\mu_E}{{R_y}^2}; \qquad \mu_E = 2\mu_s - 1 \tag{13}$$

where M* is the effective modal mass for the first mode of vibration of the building; T is the period of the demand spectrum; μ_s is the ductility factor; γ_E is the energy factor, in terms of energy ductility μ_E; R_y is the yield strength reduction factor; and Sa is the pseudo-acceleration spectrum. The values of μ_s and R_y can be easily obtained using R_y-μ_s -T equations that are evaluable in the literature [29]. In this research, the equations proposed by Chopra [32] based on the elastic design spectrum of Newmark and Hall [51] were used:

$$R_y = \begin{cases} 1 & T < T_a \\ (2\mu_s - 1)^{\frac{\beta}{2}} & T_a \le T \le T_b \\ \sqrt{2\mu_s - 1} & T_b \le T \le T_c\sqrt{2\mu_s - 1}/\mu \\ (T/T_c)\mu_s & T_c\sqrt{2\mu_s - 1}/\mu \le T \le T_c \\ \mu_s & T > T_c \end{cases} \quad (14)$$

$$\beta = \ln\left(\frac{T}{T_a}\right)\ln\left(\frac{T_a}{T_b}\right) \quad (15)$$

where Ta, Tb and Tc are limiting period values that depend on ground motion parameters. Sa_{EDRS} can be obtained based on the demand spectrum in the acceleration displacement response spectrum (ADRS) format and using Eqs. (12) to (15).

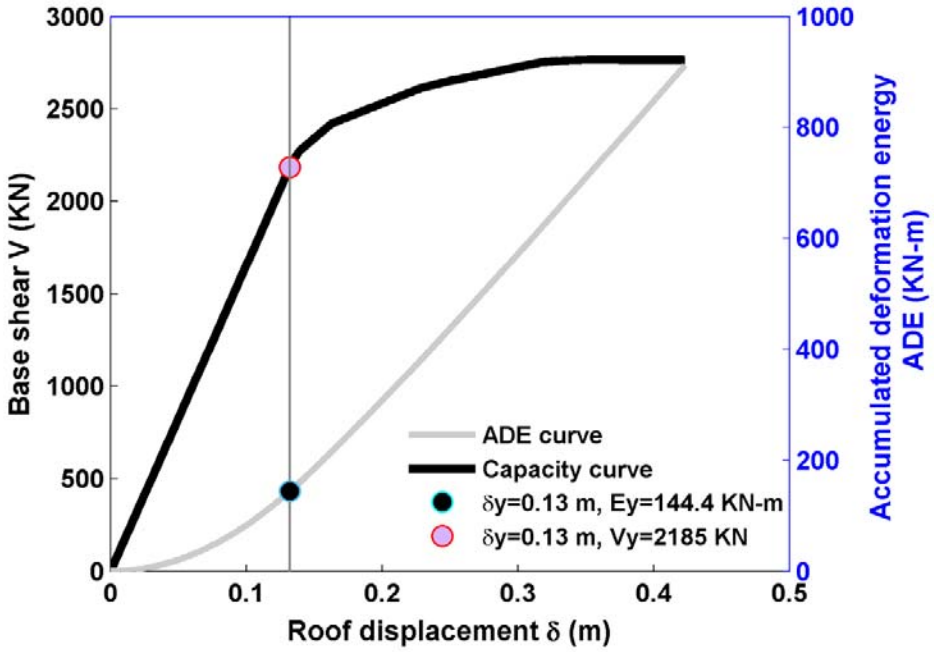

Figure 7. Capacity curve and ADE curve of the building.

In order to assure the energy balance [31,53–55], the following steps should be carried out: i) convert the roof displacement of the ADE curve to spectral displacement, Sd, using the modal participation factor, PF_1; ii) normalize the ADE curve and the spectrum of energy demand, Sa_{EDRS}, with the corresponding energy value at the yielding displacement, E_y; iii) obtain the Sa_{EDRS} for ductility, $\mu s=1$, and cross Sa_{EDRS} and ADE curves to find the performance point Sd_{PP}; iv) determine the ductility μ_{PP} of the relation Sd_{PP} with the yielding spectral displacement Sd_y; if $\mu_{PP} \le 1$, then Sd_{PP} is the displacement of performance for the seismic action and the structure performs in the linear range; if $\mu_{PP} > 1$, perform step iii) again for a higher μs and determine a new Sd_{PP} and μ_{PP}; repeat until $\mu s \approx \mu_{PP}$ with a predefined error; then the new Sd_{PP} is the displacement of performance for the seismic action that is applied and the structure performs in the nonlinear range. Finally, convert Sd_{PP} to roof displacement δ, using the modal participation

factor, PF_1. For the studied case, M*= 215.5 KN sec^2/m, δ_y=0.13 m; E_y=144.4 KN-m, PF_1= 1.29, the R_y - μs - T are taken from Eqs (14) and (15) where μs=1, Ta=1/33 s, Tb=0.125 s and Tc=0.6 s defined by Chopra [32] and soil conditions in the Mexico City. The Sa matched acc1 for a PGA equal to 0.45g was used, as shown in Figure 8a. Figure 8b shows the respective Sa matched acc1 in EDRS format and normalized to E_y.. Ta, Tb and Tc used in the R_y-μ_E-T equations (14) and (15), for the particular case studied, have provided adequate results. This is attributed to the fact that, R_y becomes constant in the R_y-μ_E-T equations for structures with middle and long periods, while its variation affects structures with short fundamental periods. For the studied structure, that has a middle period (T1= 0.63 s.), the variation of R_y does not have an important influence on the application of the energy balance. However, this may not be the case with other seismic actions and types of buildings. Therefore, it is recommended to calibrate these periods for each case.

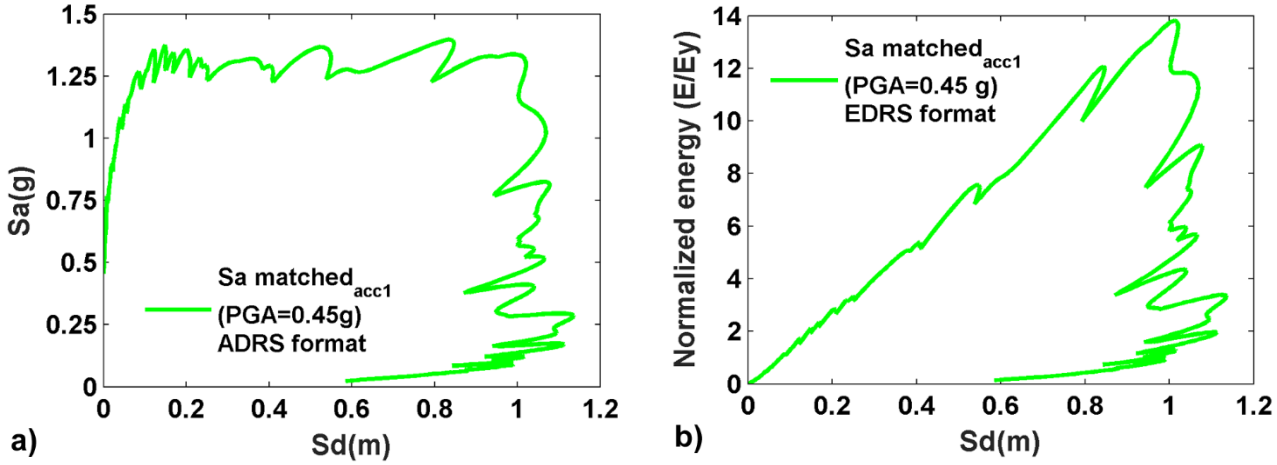

Figure 8. Sa matched acc1 for a PGA equal to 0.45 g in a) ADRS format and b) EDRS format.

Figure 9a shows an example of the energy balance for the building using $Sa_{matched}$ $acc1_{(EDRS\ format)}$ for a PGA=0.45 g and the ADE curve shown in Figure 7; both curves are normalized to E_y. For the considered values, Sd_{pp}=0.17 m and μ_s =1.64.

Static roof displacements were then determined by assuring the energy balance, considering the PGA incrementally and converting the Sd_{pp}(PGA) into roof displacements, δ(PGA). Based on the IDA of the building, the relation between PGA and the maximum roof displacement, δ is obtained. The values δ of this relation define the dynamic displacement pattern. Figure 9b shows the comparison between static and dynamic displacement functions that have been obtained using the IDA and the energy balance respectively. In this case, both displacement functions show very good agreement.

The energy functions $E_{so}(\delta)_{NN}$ and $E_D(\delta)_{NN}$ are obtained based on the static roof displacement function (see Figure 10a). The $DI_{PAw}(\delta)$ of the building is used to calibrate the energy capacity damage index to obtain η=0.70. This means that the contribution to the damage index of the strain energy function, $E_{so}(\delta)_{NN}$, is 70%, while the

contribution of the hysteretic dissipated energy, $E_D(\delta)_{NN}$, is 30%. These percentages would vary for different seismic actions.

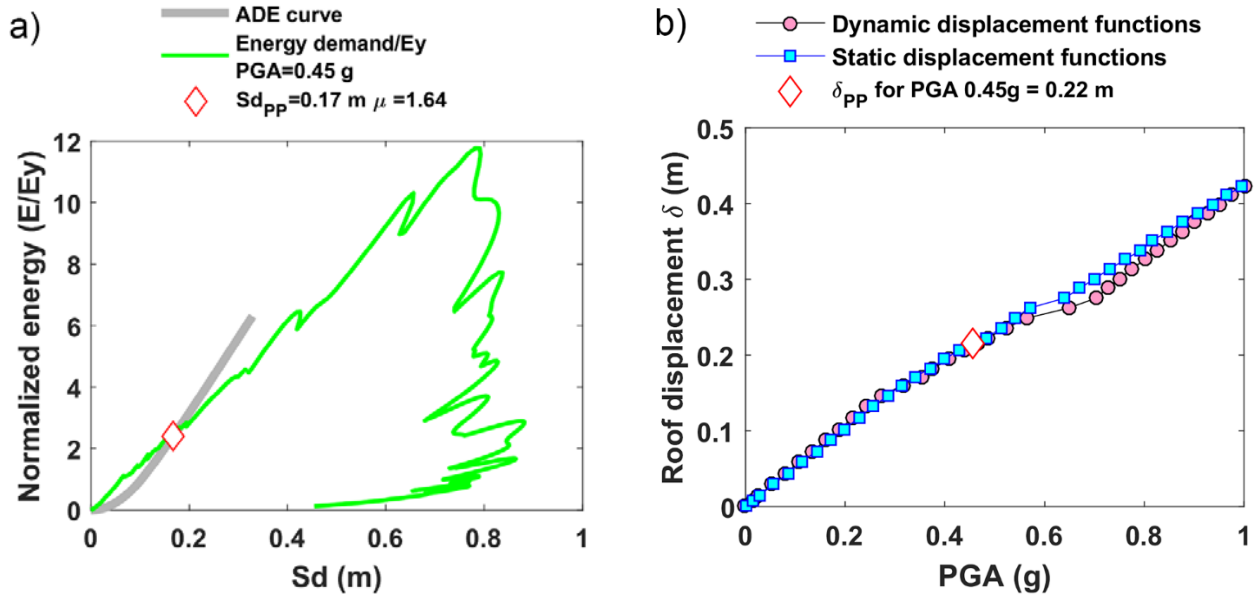

Figure 9. a) The energy balance of the building with the $Sa_{matched}$ acc1 for PGA = 0.45 g; b) static and dynamic roof displacement functions.

Figure 10a shows the energy capacity damage indices $DI_{EC}(\delta)$ and $DI_{PAw}(\delta)$ for the building. Both indices show very good agreement. Observe that the damage curves that were calculated can be also related to the PGA by considering the function shown in Figure 10b. Thus, the proposed energy capacity damage index can be directly related to an intensity measure of the earthquake. Figure 10b shows $E_{so}(PGA)_{NN}$ and $E_D(PGA)_{NN}$, $DI_{PAw}(PGA)$ and $DI_{EC}(PGA)$ functions. In the case studied here, the $DI_{EC}(PGA)$ also shows very good agreement with $DI_{PAw}(PGA)$.

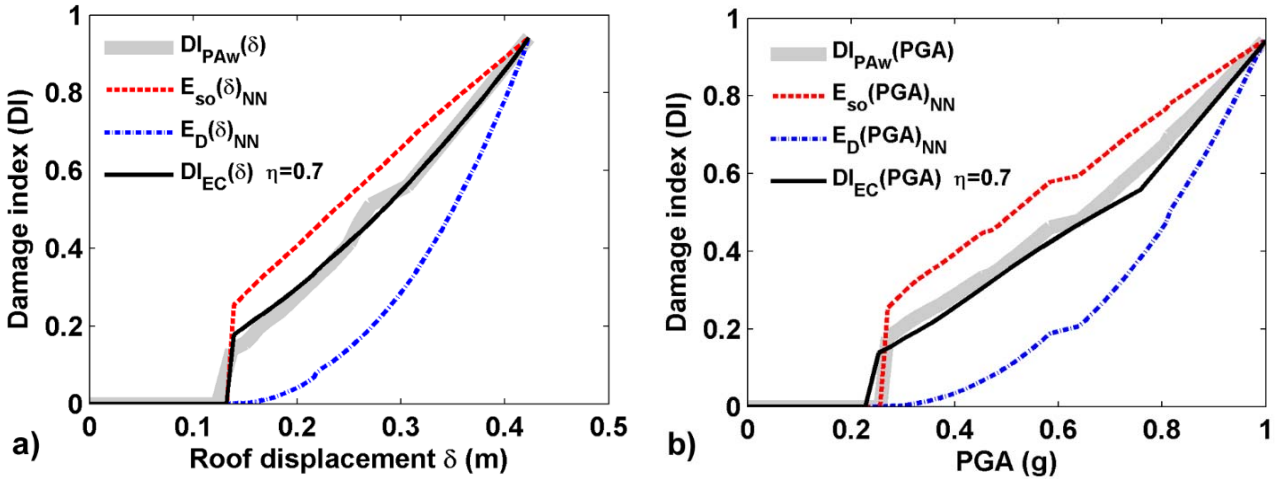

Figure 10. a) $DI_{PAw}(\delta)$ and $DI_{EC}(\delta)$; and b) $DI_{PAw}(PGA)$ and $DI_{EC}(PGA)$ of the SFM 3 building.

4 Probabilistic approach

The model of the studied building was then used to estimate the new damage index from a probabilistic perspective. It was proved that the proposed damage index fits well the results obtained with the IDA, even when several uncertainties were considered in the mechanical properties of the materials and the seismic action. For the probabilistic approach, the Monte Carlo method [56,57] and the Latin hypercube sampling (LHS) technique [58–60] were used to optimize the number of samples. The strength and ductility of the beams and columns were considered random variables in the modified Ibarra–Medina–Krawinkler (IMK) model [38–40]. The backbone curve of the modified IMK model was defined by three strength parameters (M_y= effective yield moment; M_c= capping moment strength or post-yield strength ratio M_c/M_y and M_r= $\kappa \cdot M$, residual moment) and by four deformation parameters: θ_y= yield rotation; θ_p= pre-capping plastic rotation for monotonic loading (difference between yield rotation and rotation at the maximum moment); θ_{pc}= post-capping plastic rotation (difference between rotation at maximum moment and rotation at complete loss of strength); and θ_u= ultimate rotation capacity (see Figure 11a). The strength parameters can be determined for W sections according to Lignos and Krawinkler [39,40] and from the recommendations of PEER/ATC 72-1[44] using the following equations:

$$M_y = 1.17 \cdot Z \cdot f_y \tag{16}$$

$$M_c = 1.11 \cdot M_y \tag{17}$$

$$M_r = 0.4 \cdot M_y \tag{18}$$

The deformation parameters can be determined for W sections by means of the following multi-variable empirical equations that were developed by Lignos and Krawinkler [39,40] and included in the PEER/ATC 72-1[44].

$$\theta_y = (M_y/k_o)/L = (M_y/6 \cdot E \cdot I)/L \tag{19}$$

$$\theta_p = 0.0865 \cdot \left(\frac{h}{t_w}\right)^{-0.365} \cdot \left(\frac{b_f}{2 \cdot t_f}\right)^{-0.140} \cdot \left(\frac{L}{d}\right)^{0.340} \cdot \left(\frac{c^1_{unit} \cdot d}{533}\right)^{-0.721} \cdot \left(\frac{c^2_{unit} \cdot f_y}{355}\right)^{-0.721} \quad \sigma_{In} = 0.32 \tag{20}$$

$$\theta_{pc} = 5.63 \cdot \left(\frac{h}{t_w}\right)^{-0.565} \cdot \left(\frac{b_f}{2 \cdot t_f}\right)^{-0.800} \cdot \left(\frac{c^1_{unit} \cdot d}{533}\right)^{-0.280} \cdot \left(\frac{c^2_{unit} \cdot f_y}{355}\right)^{-0.430} \quad \sigma_{In} = 0.25 \tag{21}$$

$$\theta_u = 1.5 \cdot (\theta_y + \theta_p) \tag{22}$$

In these equations, k_o is the initial elastic stiffness; I is the inertia moment; c^1_{unit} and c^2_{unit} are coefficients for units conversion; h/t_w is the ratio between the web depth and the thickness; L/d is the ratio between the span and the depth of the beam; $b_f/(2 \cdot t_f)$ is the width/thickness ratio of the beam flange; and σ_{In} is the standard deviation, assuming a lognormal fit of experimental data.

In this research, the modified IMK model of the structural sections was defined by all the strength parameters based on the expected yield strength, f_y; and the deformation parameters (ductility) based on θ_p and θ_{pc}. PEER/ATC 72-1 [44] recommends that, when experimental results of cyclic degradation of stiffness in the structural elements are not available, as in this study, the parameters θ_p and θ_{pc} should be adapted as follows: $\theta'_p=0.7\theta_p$ and $\theta'_{pc}= 0.5\theta_{pc}$.

The behavior of structural elements is described by means of the modified IMK model; this model can be implemented in Ruaumoko [2] by using the bi-linear hysteresis rule with strength reduction based on the ductility, using the following equations:

$$r=\left[\frac{M_c-M_y}{\theta'_p}\right]/k_o \tag{23}$$

$$DUCT1=\frac{\theta_y+\theta'_p}{\theta_y} \tag{24}$$

$$DUCT2=\frac{\theta_y+\theta'_p+\left[\theta'_{pc}(M_c-M_r)/M_c\right]}{\theta_y} \tag{25}$$

$$DUCT3=\frac{\theta_y+\theta'_p+\theta'_{pc}}{\theta_y} \tag{26}$$

where r is hardening factor as a fraction of the initial stiffness, k_o. DUCT1 is the ductility at which degradation begins. DUCT2 is the ductility at which degradation ends. The strength reduction rule in Ruaumoko program indicates that, DUCT2 is based on the residual strength of the element by means of the constant, RDUCT. In this article, RDUCT was defined by means of the constant k = 0.4 of the modified IMK model. Finally, DUCT3 is the ductility at 0.01 of the initial strength [2]. Thus, using equations (16) to (26), the expected performance of the structural elements was modelled in Ruaumoko. Figure 11a shows the model used herein based on the parameters of the modified IMK model, and the bi-linear hysteresis rule with strength reduction based on the ductility as defined in Ruaumoko.

For a better representation of physical randomness in the problem, for each structural element, a random sample of the three parameters (f_y, θ_p and θ_{pc}) was generated. Then, the properties of strength and ductility of the plastic hinges of each element were estimated. It was assumed that the hinges at both ends of the elements were the same. Thus, the 3-storey model with 27 elements (15 columns and 12 beams) had 81 random variables. Table 2 shows the mean value μ, the standard deviation, the coefficient of variation (COV) and the assumed probability distributions of these 3 parameters.

Moreover, to avoid unrealistic samples in LHS simulations, the normal distribution of f_y and lognormal distributions of θ_p and θ_{pc} were truncated at both ends. The lower and upper limits were determined by the mean value ± 2 standard deviations ($\mu \pm 2\sigma$). The purpose of this truncation was to avoid under- or overestimates of the capabilities of the elements with samples without physical meaning.

In summary, for this research, a simplified probabilistic approach was proposed. The method used the modified IMK model for beams and columns, and uncertainties were concentrated on the variables f_y, θ_p and θ_{pc}. Thus, it was assumed that these three variables have a major influence on the linear and nonlinear structural response of buildings. Besides, the use of these variables is recommended in the new codes for probabilistic seismic performance assessment of steel buildings [44,61].

Another important sampling issue is the correlation among variables. Two types of correlations were considered in this research: intra- and inter-element. The intra-element correlation was given by the relation among the three parameters simulated for the same hinge; these correlations can be derived from Eqs. (20) and (21) [39,40] and are defined in Table 3. The inter-element was defined based on research conducted by Idota et al. [62] and Kazantzi et al. [63] on consistency in workmanship and material quality between different steel structural W sections. An inter-element correlation of 0.65 was used herein for the same section type, and a null correlation was assumed for different sections.

Table 2. Probabilistic property of strength and ductility random variables.

Structural section	Type	Variable	Mean (μ)	Standard deviation (σ or σ_{ln})	Function
W14X68	Strength	f_y	375.76 MPa*	26.68 MPa (COV=0.071*)	Normal distribution
	Ductility	θ_p	0.054 rad♦	σ_{ln} =0.32♦	Lognormal distribution
	Ductility	θ_{pc}	0.188 rad♦	σ_{ln} =0.25♦	Lognormal distribution
W16X89	Strength	f_y	375.76 MPa*	26.68 MPa (COV=0.071*)	Normal distribution
	Ductility	θ_p	0.047 rad♦	σ_{ln} =0.32♦	Lognormal distribution
	Ductility	θ_{pc}	0.210 rad♦	σ_{ln} =0.25♦	Lognormal distribution
W18X97	Strength	f_y	375.76 MPa*	26.68 MPa (COV=0.071*)	Normal distribution
	Ductility	θ_p	0.044 rad♦	σ_{ln} =0.32♦	Lognormal distribution
	Ductility	θ_{pc}	0.183 rad♦	σ_{ln} =0.25♦	Lognormal distribution

* Based on the report by Lignos & Krawinkler [39] for statistics of material yielding strength, obtained from flanges-webs tests for A572 grade steel.
♦ For the steel, structural W sections were determined by means of the multi-variable empirical Equations (20) and (21).

Table 3. Intra-element correlation for random variables of beams and columns.

	f_y	θ_p	θ_{pc}
f_y	1	0	0
θ_p	0	1	0.69
θ_{pc}	0	0.69	1

In order to assess the seismic behaviour of the building in a probabilistic environment, 200 NLSAs and 200 NLDAs were performed using the same structural models for both the static and dynamic analysis. Figure 11b shows an example of the modified IMK model used in the 12-beam W14x68 section of the probabilistic models.

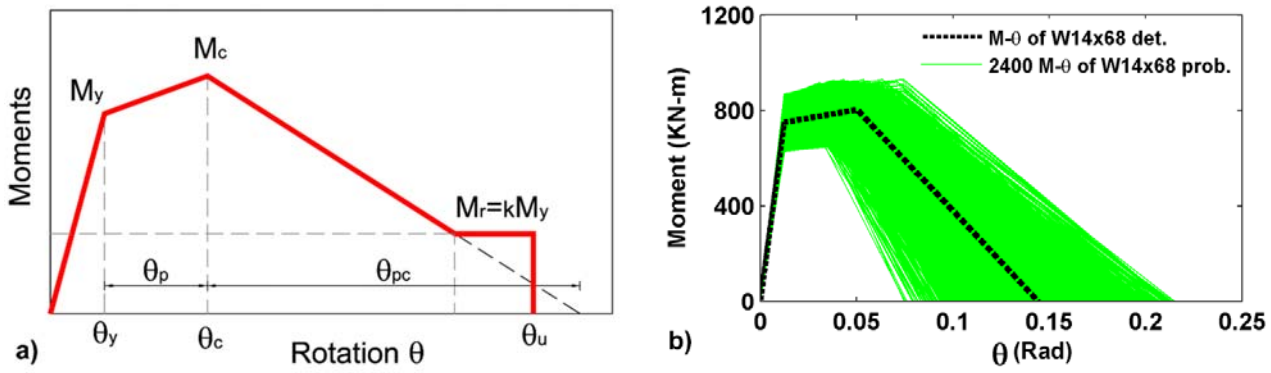

Figure 11. (a) Modified IMK model: monotonic curve; (b) an example of the modified IMK model used in the structural section (W14x68) of the probabilistic models.

Seismic action was also considered in a probabilistic way using the set of 20 matched accelerograms developed in Section 3.2 and their corresponding response spectra shown in Figure 12. The mean of the 20 response spectra accurately represents the target spectrum of the study area (Mexico City). Figure 12 also shows the fundamental period variation of the probabilistic models, $T1_{SFM3}$ prob. For each of the probabilistic IDA, one of the 20 available records was randomly selected, using a uniform probability distribution.

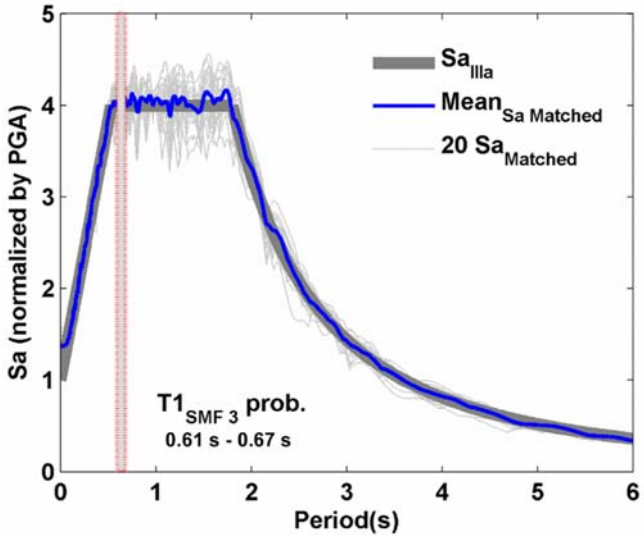

Figure 12. Response spectra of the 20 matched accelerograms and the mean spectrum. The fundamental periods of the probabilistic models are also depicted.

Figure 13a shows the probabilistic capacity curves obtained using the procedure explained in Section 3.3, and the curve representing the 50th percentile (median) of the curves. Figure 13b shows the corresponding ADE curves calculated from the capacity curves depicted in Figure 13a. Figure 14a shows the probabilistic $DI_{PAw}(\delta)$ and Figure 14b the probabilistic $DI_{PAw}(PGA)$, both obtained with IDA analysis, in accordance with the procedure explained in Section 3.4. Their respective 50th percentiles (medians) are also depicted.

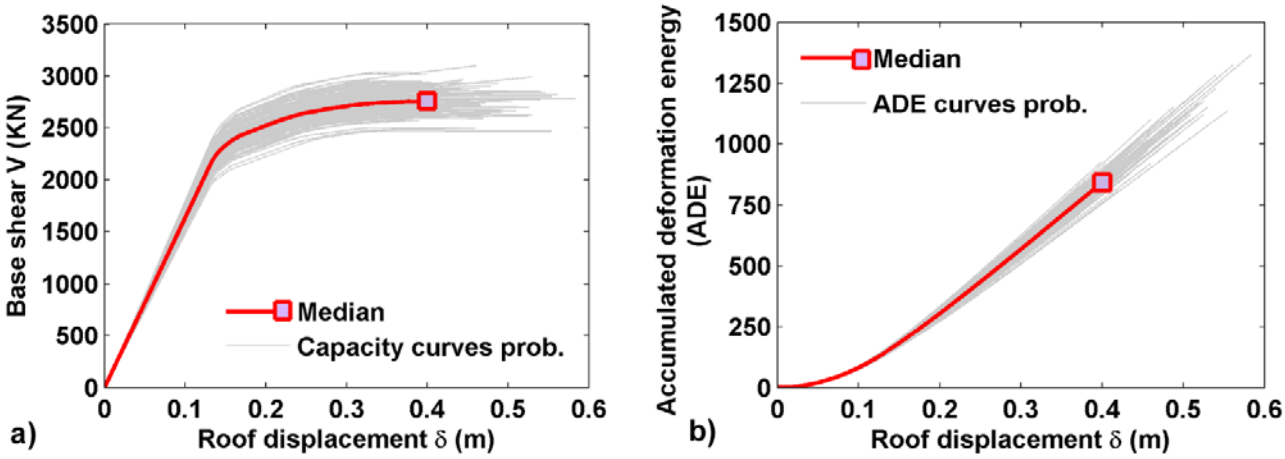

Figure 13. a) Probabilistic capacity curves and b) the respective ADE curves of the building.

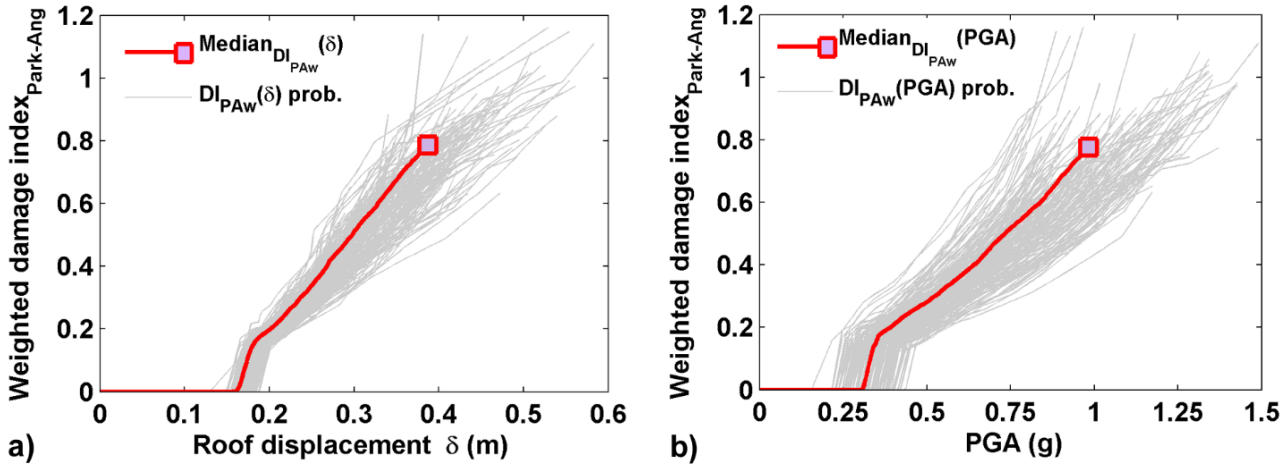

Figure 14. a) The $DI_{PAw}(\delta)$ probabilistic curve and b) the $DI_{PAw}(PGA)$ probabilistic curve.

The static displacement function of each probabilistic model was determined based on the energy balance between its ADE curve and the response spectrum in EDRS format of the matched accelerogram that was used in the IDA in the same probabilistic model.

Then, the energy capacity damage index, $DI_{EC}(\delta)$, was calculated and calibrated with the corresponding $DI_{PAw}(\delta)$. Figure 15a shows the curves that were obtained. In this figure, the $DI_{PAw}(\delta)$ curves calculated via IDA are shown together with the corresponding $DI_{EC}(\delta)$ curves. The median curves are also shown in Figure 15a. The median $DI_{EC}(\delta)$ curve shows a good fit with the median $DI_{PAw}(\delta)$ curve for parameter η=0.62. Therefore, for probabilistic cases, the contribution to the $DI_{EC}(\delta)$ of the strain energy function, $E_{so}(\delta)_{NN}$, is 62%, while the contribution of the energy dissipated by hysteretic cycles, $E_D(\delta)_{NN}$, is 38%. The $DI_{EC}(\delta)$ can be well fitted to the $DI_{PAw}(\delta)$. Figure 15b shows the $DI_{PAw}(PGA)$ and the $DI_{EC}(PGA)$ probabilistic functions. Again, in all cases, the agreement was very good, especially in the median value. Therefore, the new damage index can also be used to establish the expected damage in function of the intensity of the seismic action.

Finally, parameter η is crucial in the energy damage index. Note that each $DI_{PAw}(\delta)$ curve is obtained for a specific seismic action. Different seismic actions can be expected to lead to different Park and Ang index values and, therefore, to different values of the parameter η. Thus, parameter η allows the new index, $DI_{EC}(\delta)$, to fit the response and the expected damage properly when the building is subjected to different seismic actions.

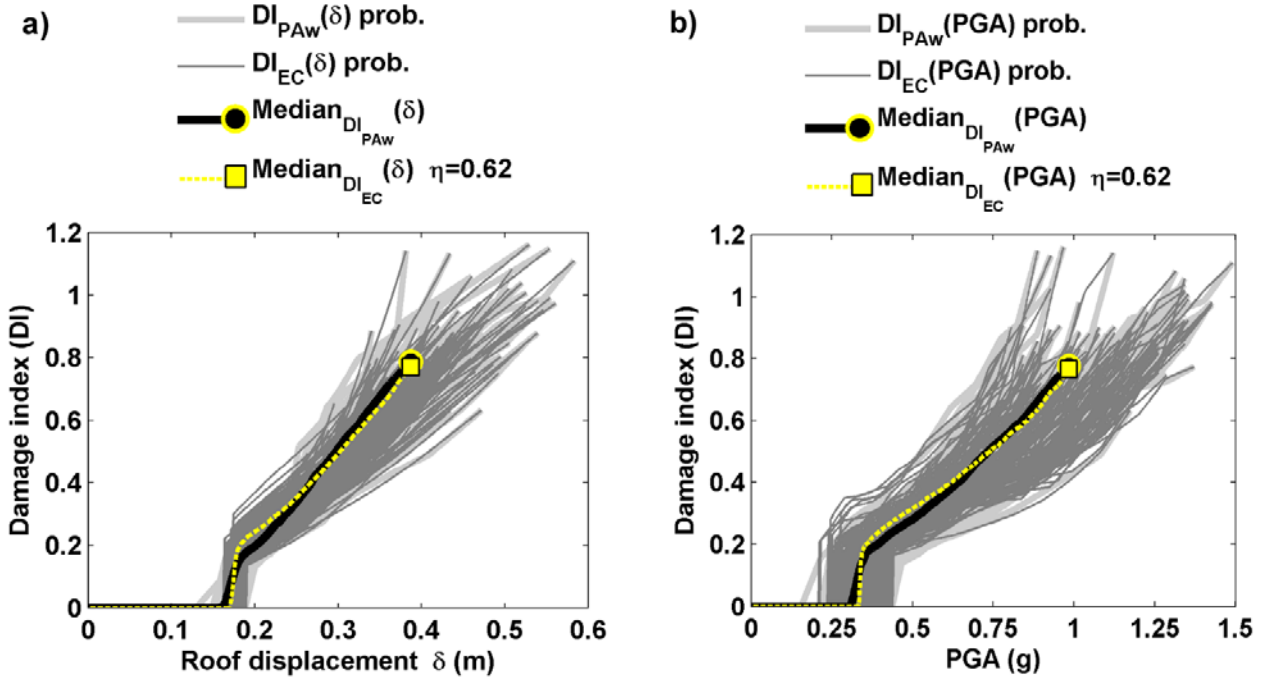

Figure 15. a) The $DI_{PAw}(\delta)$ and the $DI_{EC}(\delta)$ probabilistic curves, and b) the $DI_{PAw}(PGA)$ and the $DI_{EC}(PGA)$ probabilistic curves.

5 Discussion and conclusions

5.1 Overview

Based on the capacity curve obtained by nonlinear static analysis, a new damage index has been developed in this research, Two energy functions have been defined. The former is strain energy, $E_{so}(\delta)$, which is associated with stiffness variation and the ductility of the structure. The latter is the energy dissipated by damping, $E_D(\delta)$, which is related to the energy dissipated by hysteretic cycles. Using a linear combination of these two energy functions by means of a parameter of contribution to damage η, the new damage index, $DI_{EC}(\delta)$, has been defined. Parameter η has been calibrated using the well-known Park and Ang damage index, $DI_{PAw}(\delta)$, which is obtained from IDA. Both damage indices show good agreement.

5.2 Discussion

The main objective of this research has been to implement a simplified damage index, $DI_{EC}(\delta)$, applied to steel buildings. For this index, the energy balance method, which has been applied incrementally, has determined the static displacement pattern in the studied building under the applied seismic actions. $DI_{EC}(\delta)$ can be expressed in

terms of the increase of PGA, $DI_{EC}(PGA)$. The advantage of $DI_{EC}(PGA)$ is that it provides a scenario of expected damage, based on the characteristics of the seismic action to which the building is subjected. This result is similar to the damage scenario obtained with IDA.

The distribution parameter, η, depends on the characteristics of the seismic action. That is, different seismic actions would lead to different $DI_{PAw}(\delta)$ and, therefore, to different values of the parameter η. For instance, longer duration of the earthquake would produce a larger contribution of the energy function linked to the hysteresis, which makes parameter η lower, when $DI_{EC}(\delta)$ is fitted. It would be interesting to evaluate the sensitivity of parameter η for seismic actions with different response spectra and different earthquake durations. The relation between the parameter η and the type of frame for different buildings may be also studied.

It is clear that, if the new damage index needs to be calibrated for each new building and for each different seismic action, the advantages of this simplified damage index vanish. Ongoing research shows that values of parameter η are very stable. Values in the range 0.6-0.7 are obtained. Values in the low part of the range (around 0.6) are obtained for long duration seismic actions. On the contrary, high values (around 0.7) are obtained for impulsive near-fault short accelerograms. Moreover, similar values are obtained for reinforced concrete and for steel buildings. However, these are preliminary results and further research is needed to support them. Therefore, accurate calibrations of this parameter η, can lead to tabulated values for different seismic actions and building types. In this paper, the new simple damage index has been presented; more detailed work to obtain tabulated values for selected seismic actions and building types is beyond the purpose of this work.

Because the new damage index is calibrated so that it is equivalent to the Park and Ang damage index, it does not improve the quantitative damage assessment but, if tabulated values of the parameter η are available, the new damage index can be used in a quick, straightforward and routine way.

5.3 Conclusions

Several relevant conclusions of this research are the following:

- The new damage index, $DI_{EC}(\delta)$, based on two energy functions can be obtained directly from the capacity curves in a straightforward way, and provides adequate results for assessing expected damage in buildings, as a function of the characteristics of the applied seismic action, such as for instance, the frequency content and duration.
- The energy balance method applied incrementally is a good technique to estimate the static displacement pattern and these displacements are used in such a way that the $DI_{EC}(\delta)$ can be obtained also as a function of the intensity of the applied seismic action, that is, $DI_{EC}(PGA)$ in this case.
- The parameter η is crucial in the new damage index, as it separates the contribution of the strain energy, $E_{so}(\delta)$, from that of the energy dissipated by hysteretic cycles, $E_D(\delta)$.

- Concerning the damage index for the buildings and the seismic actions studied in this research, on average, the Park and Ang damage index is well fitted by the combination of 62% of the $E_{so}(\delta)$ function and 38% of the $E_D(\delta)$ function.

The results of this research show that, the $DI_{EC}(\delta$ or PGA) can be a useful tool to evaluate the seismic damage of buildings, especially in a probabilistic environment in which computational times can be significantly reduced.

6 Notations

The following symbols were used in this paper:

Ac	=	Area under the capacity curve.
acc	=	Accelerograms.
ADE(δ)	=	Accumulated deformation energy of the capacity curve.
$b_f/(2\cdot t_f)$	=	Width/thickness ratio of the beam flange of W section.
COV	=	Coefficient of variation of the probabilistic variables.
c^1_{unit} and c^2_{unit}	=	Coefficients for units conversion in the modified IMK model.
D_{bi}, F_{bi}	=	Coordinates of the ultimate capacity point of the bilinear curve.
D_{ci}, F_{ci}	=	Coordinates of the ultimate capacity point of the capacity curve.
$DI_{EC}(\delta)$, $DI_{EC}(\theta)$ or $DI_{EC}(PGA)$	=	Energy capacity damage index in function of the roof displacement, rotation and PGA, respectively.
$DIe_{PA}(\delta)$ or $DIe_{PA}(\theta)$	=	Park and Ang damage index of a structural element.
$DI_{PAw}(\delta)$, $DI_{PAw}(\theta)$ or $DI_{PAw}(PGA)$	=	Park and Ang damage index of a building in function the roof displacement, rotation and PGA, respectively.
$\int_0^\delta dE$	=	Hysteretic energy absorbed by the element during the earthquake.
D_y, F_y	=	Coordinates of the yield point of the bilinear curve.
E	=	Modulus of elasticity.
EDRS	=	Energy Displacement Response Spectrum.
E_D	=	Energy dissipated by the structure in a single cycle of motion.
$E_D(\delta)$	=	Energy dissipated function.
$E_D(\delta)_{NN}$, $E_D(\theta)_{NN}$ or $E_D(PGA)_{NN}$	=	Normalized energy dissipated in function of the roof displacement, rotation or PGA, respectively.
E_{so}	=	Maximum strain energy associated to a cycle of motion.
$E_{so}(\delta)$	=	Strain energy function.
$E_{so}(\delta)_{NN}$, $E_{so}(\theta)_{NN}$ or $E_{so}(PGA)_{NN}$	=	Normalized strain energy in function of the roof displacement, rotation or PGA, respectively.
E_y	=	Yielding energy.
F(δ)	=	Capacity curve.
FR	=	Connections type Fully Restrained.
f_y	=	Expected yield strength.
h/t_w	=	Ratio between the web depth and the thickness of W section.
i	=	Structural element *i*.
I	=	Inertia moment of W section.
IDA	=	Incremental dynamic analysis.
IMK	=	Modified Ibarra–Medina–Krawinkler model.
j	=	Each increment in the displacement of the capacity curve.
k	=	Residual moment constant.
Ki	=	Initial slope of the capacity curve.
k_o	=	Initial elastic stiffness.
L/d	=	The ratio between the span and the depth of the beam or column.
LHS	=	Latin Hypercube Sampling.
M	=	Bending moment in the structural element.

M_c	=	Capping moment strength or post-yield strength ratio.
M_r	=	Residual moment.
M_w	=	Moment magnitude scale.
M_y	=	Effective yield moment.
M*	=	Effective modal mass for the first mode of vibration of the building.
N	=	Number of damaged structural elements in the building.
n	=	Ultimate increment in the displacement of the capacity curve.
NLDA	=	Nonlinear dynamic analysis.
NLSA	=	Nonlinear static analysis.
PA	=	Park and Ang damage index.
P_{ad}	=	Adaptive pushover analysis.
PF_1	=	Modal participation factor.
PGA	=	Peak ground acceleration.
Qu	=	Strength corresponding to the ultimate displacement.
Qy	=	Strength at the yielding point.
R_y	=	Strength reduction factor.
Sa	=	Acceleration spectrum.
Sa_{EDRS}	=	Input energy spectrum.
$Sa_{matched}$	=	Acceleration spectrum of the matched accelerogram.
Sd		Spectral displacement in the structure.
Sd_{pp}	=	Spectral displacement of the performance point.
Sd_y	=	Yielding spectral displacement.
SMF	=	Special moment frame building.
Sv	=	Velocity spectrum.
T	=	Structural period.
T_a, T_b and T_c	=	Limit periods used to define the Ry-μ_s-T relationship.
T_1	=	Fundamental period of the building.
$T1_{SFM3}$ prob	=	The fundamental period of the probabilistic models SMF 3.
V	=	Base shear in the structure.
V_y	=	Base shear in the yielding energy.
Z	=	Plastic modulus.
β	=	Strength deteriorating parameter in the Park and Ang damage index.
β*	=	Parameter of the Ry in function of the T_a, T_b and T_c.
γ_E	=	Energy factor.
δ	=	Roof displacement in the structure.
δ_{Dy}	=	Displacement in the yielding point of the bilinear curve.
δ_u	=	Ultimate roof displacement in the structure.
δ_y	=	Roof displacement in the yielding energy.
η	=	Calibration parameter in the energy capacity damage index.
θ	=	Rotation in the structural element.
θ_p	=	Pre-capping plastic rotation for monotonic loading.
θ_{pc}	=	Post-capping plastic rotation.
θ_u	=	Ultimate rotation capacity.
θ_y	=	Yield rotation.
λ_i	=	Ratio of the energy dissipated by hysteresis in the element *i* to the total hysteretic energy dissipated in the entire building.
μ	=	Mean value of the probabilistic variables.
μ_E	=	Energy ductility.
μ_{PP}	=	Ductility of the performance point.
μ_s	=	Ductility factor.
ξ_{eq},	=	Equivalent viscous damping.
σ	=	Standard deviation of the probabilistic variables.
σ_{In}	=	Standard deviation, assuming a lognormal fit of experimental data in θ_p and θ_{pc} in the modified IMK model.
ω	=	Tangent fundamental natural frequency in the modified Rayleigh method.

7 Acknowledgements

This research was partially funded by the Ministry of Economy and Competitiveness (MINECO) of the Spanish Government and by the European Regional Development Fund (ERDF) of the European Union (EU) through projects referenced as: CGL2011-23621 and CGL2015-65913-P (MINECO/FEDER, UE). The first author holds PhD fellowships from the Universidad Juarez Autonoma de Tabasco (UJAT) and from the 'Programa de Mejoramiento del Profesorado, Mexico (PROMEP)'.

8 References

[1] Vamvatsikos D, Cornell CA. Incremental dynamic analysis. Earthq. Eng. Struct. Dyn. 2002; 31 (3):491–514.

[2] Carr AJ. Ruaumoko 2d y 3d Inelastic Dynamic Analysis Program (Version 2007) [Software]. University of Canterbury, Christchurch, New Zealand. 2002; http://www.civil.canterbury.ac.nz/ruaumoko

[3] Kamaris GS, Hatzigeorgiou GD, Beskos DE. A new damage index for plane steel frames exhibiting strength and stiffness degradation under seismic motion. Eng. Struct. 2013; 46:727–736.

[4] Cosenza E, Manfredi G, Ramasco R. The use of damage functionals in earthquake engineering: a comparison between different methods. Earthq. Eng. Struct. Dyn. 1993; 22:855–868.

[5] Powell GH, Allahabadi R. Seismic damage prediction by deterministic methods: Concepts and procedures. Earthq. Eng. Struct. Dyn. 1988; 16(5):719-734.

[6] Bracci JM, Reinhorn AM, Mander JB, Kunnath SK. Deterministic model for seismic damage evaluation of reinforced concrete structures. Technical Report NCEER-89–0033, National Center for Earthquake Engineering Research, State University of New York at Buffalo. 1989.

[7] Bojorquez E, Reyes-Salazar A, Teran-Gilmore A, Ruiz SE. Energy-based damage index for steel structures. Steel Compos. Struct. 2010; 10(4):331-348.

[8] Krawinkler H, Zohrei M. Cumulative damage in steel structure subjected to earthquake ground motions. Comput. Struct. 1983; 16(1-4):531-541.

[9] DiPasquale E, Cakmak AS. Seismic damage assessment using linear models. Soil Dyn. Earthq. Eng. 1990; 9(4):194-215.

[10] Banon H, Veneziano D. Seismic safety of reinforced concrete members and structures. Earthq. Eng. Struct. Dyn. 1982; 10(2):179-193.

[11] Park YJ, Ang AH-S. Mechanistic seismic damage model for reinforced concrete. ASCE J Struct. Eng. 1985; 111(4):722–739.

[12] Roufaiel MSL, Meyer C. Analytical modeling of hysteretic behavior of R/C Frames. J. Struct. Eng. ASCE. 1987; 113(3):429-457.

[13] Bozorgnia Y, Bertero V. Improved shaking and damage parameters for post-earthquake applications. In: Proceedings, SMIP01 Seminar on Utilization of Strong-Motion Data, Los Angeles. 2001; p. 22

[14] Málaga-Chuquitaype C, Elghazouli AY. Evaluation of fatigue and Park and Ang damage indexes in steel structures. In: Proc. 15thWorld Conf. Earthq. Eng. Lisbon Portugal. 2012.

[15] Kostinakis K, Athanatopoulou A, Morfidis K. Correlation between ground motion intensity measures and seismic damage of 3D R/C buildings. Eng. Struct. 2015; 82:151–167.

[16] Vargas YF, Pujades LG, Barbat AH, Hurtado JE. Probabilistic seismic damage assessment of RC buildings based on nonlinear dynamic analysis. The Open Civil Engineering Journal. 2015; 9(Suppl. 1, M 12): 344-350.

[17] Mwafy A, Elnashai A. Static pushover versus dynamic collapse analysis of RC buildings. Eng. Struct. 2001; 23(5):407–424.

[18] Kim SP, Kurama YC. An alternative pushover analysis procedure to estimate seismic displacement demands. Eng. Struct. 2008; 30(12):3793–3807.

[19] Fragiadakis M, Vamvatsikos D. Fast performance uncertainty estimation via pushover and approximate IDA. Earthq. Eng. Struct. Dyn. 2010; 39: 683-703.

[20] Celarec D, Dolšek M. The impact of modelling uncertainties on the seismic performance assessment of reinforced concrete frame buildings. Eng. Struct. 2013; 52(1):340–354.

[21] Vargas YF, Pujades LG, Barbat AH, Hurtado JE. Capacity, fragility and damage in reinforced concrete buildings: A probabilistic approach. Bull. Earthq. Eng. 2013; 11(6):2007–2032.

[22] Pujades LG, Vargas-Alzate YF, Barbat AH, González-Drigo JR. Parametric model for capacity curves. Bull. Earthq. Eng. 2015; 13(5):1347–1376.

[23] Barbat AH, Vargas YF, Pujades LG, Hurtado JE. Evaluación probabilista del riesgo sísmico de estructuras con base en la degradación de rigidez. Rev Int Metod Numéricos Para Cálculo Y Diseño en Ing. 2016; 32(1):39-47.

[24] Lantada N, Irrizari J, Barbat AH, Goula X, Roca A, Susagna T and Pujades LG. Seismic hazard and risk scenarios for Barcelona, Spain, using the Risk-UE vulnerability index method. Bull. Earthq. Eng. 2010; 8:201-229.

[25] Barbat AH, Carreño ML, Cardona OD, Marulanda MC. Evaluación holística del riesgo sísmico en zonas urbanas. Rev Int Metod Numéricos Para Cálculo Y Diseño en Ing. 2011; 27(1):3-27.

[26] Pujades LG, Barbat AH, Gonzalez-Drigo R, Avila J, Lagomarsino S. Seismic performance of a block of buildings representative of the typical construction in the Eixample district in Barcelona (Spain). Bull. Earthq. Eng. 2012; 10(1):331–349.

[27] Gonzalez-Drigo R, Avila-Haro J, Pujades LG, Barbat AH. Non-linear static procedures applied to high-rise residential URM buildings. Bull. Earthq. Eng. 2017; 15(1):149-174.

[28] ATC-40. Seismic evaluation and retrofit of concrete buildings. Applied Technology Council. Redwood City, California. 1996; p. 346.

[29] Chopra AK, Goel RK. Capacity-demand-diagram methods based on inelastic design spectrum. Earthq. Spectra. 1999; 15(4):637 655.

[30] Housner, GW. The plastic failure of frames during earthquakes, in: 2nd World Conference on Earthquake Engineering. 1960; pp. 997–1012.

[31] Leelataviwat S, Saewon W, Goel SC. Application of energy balance concept in seismic evaluation of structures. J. Struct. Eng. ASCE. 2009; 135(2):113-121

[32] Chopra AK. Dynamics of structures: theory and applications to earthquake. Chaps. 3. Englewood Cliffs, New Jersey: Prentice Hall. 1995; p. 944.

[33] Diaz SA, Pujades LG, Barbat AH, Gonzalez-Drigo JR, Hidalgo-Leiva DA. Capacity parametric model and damage index for steel buildings. A probabilistic approach. In: 16th World Conference of Earthquake Engineering (16WCEE) Santiago, Chile. 2017; paper number 0013.

[34] Diaz SA, Pujades LG, Barbat AH, Hidalgo-Leiva DA, Vargas-Alzate YF. Análisis dinámico probabilista de edificios de acero sometidos a sismos de larga duración. Revista Internacional de Métodos Numéricos para el Cálculo y Diseño en Ingeniería. 2017. DOI: 10.23967/j.rimni.2017.5.004.

[35] ANSI/AISC 358. Prequalified connections for special and intermediate steel moment frames for seismic applications. American Institute of Steel Construction. 2010; p. 178.

[36] NTC-DF. Norma técnica complementaria del Distrito Federal. Technical Report Gaceta oficial del Distrito Federal, México. Tomo I y II. 2004; p. 586.

[37] ANSI/AISC 341-10. Seismic provisions for structural steel buildings. An American National Standard and American Institute of Steel Construction. 2010; 356 pp.

[38] Ibarra LF, Medina RA, Krawinkler H. Hysteretic models that incorporate strength and stiffness deterioration. Earthq. Eng. Struct. Dyn. 2005; 34(12):1489–1511.

[39] Lignos DG, Krawinkler H. Deterioration modeling of steel components in support of collapse prediction of steel moment frames under earthquake loading. J. Struct. Eng. ASCE. 2011; 137(11):1291-1302.

[40] Lignos DG, Krawinkler H. Development and utilization of structural component databases for performance-based earthquake engineering. J. Struct. Eng. ASCE. 2013; 139(8):1382–1394.

[41] Krawinkler H. Shear design of steel frame joints. J. Struct. Eng. ASCE. 1978; 15(3):82-91.

[42] FEMA 355C. State of the art report on system performance of steel moment frames subject to earthquake ground shaking. SAC Joint Venture Partnership for the Federal Emergency Management Agency. Washington, D.C. 2000; p. 334.

[43] SAC. Analytical and field investigations of buildings affected by the Northridge earthquake of January 17, 1994. Report No. SAC-95-04, prepared by SAC Joint Venture, a partnership of SEAOC, ATC and CUREE. 1995; Available at: http://www.sacsteel.org/library/reports/sum95-04.html (last visited: 2017.02.17).

[44] PEER/ATC 72-1. Modeling and acceptance criteria for seismic design and analysis of tall buildings. Applied Technology Council and Pacific Earthquake Engineering Research Center. 2010; p. 242.

[45] Diaz SA, Pujades LG, Barbat AH, Félix JL. Efecto de la direccionalidad en la amenaza sísmica de la Ciudad de México. In: 20th Congreso Nacional de Ingeniería Sísmica. México. Acapulco, Guerrero. 2015; ISSN: 2448-5721.

[46] Hancock J, Watson-Lamprey J, Abrahamson N, Bommer J, Markatis A, McCoy E, Mendis R. An improved method of matching response spectra of recorded earthquake ground motion using wavelets. Journal of Earthquake Engineering. 2006; 10(Special issue):67-89.

[47] Freeman SA. The capacity spectrum method as a tool for seismic design. In: Proceedings of the 11th European conference on earthquake engineering. Paris. 1998.

[48] FEMA 273. NEHRP guidelines for the seismic rehabilitation of buildings, FEMA 273; and NEHRP commentary on the guidelines for the seismic rehabilitation of buildings, FEMA 274. Washington, D.C.: Federal Emergency Management Agency. 1997; p. 435.

[49] Fajfar P. Capacity spectrum method based on inelastic demand spectra. Earthq. Eng. Struct. Dyn. 1999; 28(9):979–993.

[50] Fajfar P. A nonlinear analysis method for performance-based seismic design. Earthq. Spectra. 2000; 16(3):573–592.

[51] Newmark NM, Hall WJ. Earthquake spectra and design. Earthquake Engineering Research Institute. Berkeley, California. USA. 1982; p. 103.

[52] Vidic T, Fajfar P, Fischinger M. Consistent inelastic design spectra: strength and displacement. Earthq. Eng. Struct. Dyn. 1994; 23(5):507–521.

[53] Mezzi M, Comodini F, Lucarelli M, Parducci A, Tomassoli E. Pseudo-energy response spectra for the evaluation of the seismic response from pushover analysis. In: Proc. First European Conference on Earthquake Engineering and Seismology, Switzerland. 2006; paper number 1183.

[54] Leelataviwat S, Saewon W, Goel SC. An energy based method for seismic evaluation of structures. In: Proceedings of the 14thWorld Conf. Earthq. Eng., Beijing, China. 2008.

[55] Parducci A, Comodini F, Lucarelli M, Mezzi M, Tomassoli E. Energy-based non-linear static analysis. In: Proc. First European Conference on Earthquake Engineering and Seismology. Geneva, Switzerland. 2006; paper number 1178.

[56] Hurtado JE, Barbat AH. Monte Carlo Techniques. In Computational Stochastic Mechanics. Arch Comput Methods Eng. 1998; 5(1):3–29.

[57] Rubinstein RY. Simulation and the Monte Carlo method, John Wiley. New York. 1981; p. 372.

[58] McKay MD, Conover WJ, Beckman R. A comparison of three methods for selecting values of input variables in the analysis of output from a computer code. J. Technometrics. 1979; 21(2):239–245.

[59] Iman RL Appendix A:Latin Hypercube Sampling. Encyclopedia of Statistical Sciences, Update Volume 3, Wiley, NY. 1999: 408-411.

[60] Vamvatsikos D. Seismic performance uncertainty estimation via IDA with progressive accelerogram-wise Latin Hypercube Sampling. J. Struct. Eng. ASCE. 2014; 140(8):1–10.

[61] FEMA P-58-1. Seismic performance assessment of buildings Vol. 1 and Vol. 2. SAC Joint Venture Partnership for the Federal Emergency Management Agency. Washington, D.C. Vol 1. 2012; p. 278.

[62] Idota H, Guan L, Yamazaki K. Statistical correlation of steel members for system reliability analysis. In: Proceedings of the 9th international conference on structural safety and reliability (ICOSSAR). Osaka, Japan. 2009.

[63] Kazantzi AK, Vamvatsikos D, Lignos DG. Seismic performance of a steel moment-resisting frame subject to strength and ductility uncertainty. Eng. Struct. 2014; 78:69–77.